HHS Public Access

Author manuscript

Traffic. Author manuscript; available in PMC 2017 September 01.

Published in final edited form as:

Traffic. 2016 September ; 17(9): 1027–1041. doi:10.1111/tra.12418.

Rab11 Regulates the Mast Cell Exocytic Response

Joshua D. Wilson, **Sarah A. Shelby**, **David Holowka**, and **Barbara Baird**

Department of Chemistry and Chemical Biology, Cornell University, Ithaca, NY 14853-1301

Abstract

Stimulated exocytic events provide a means for physiological communication and are a hallmark of the mast cell-mediated allergic response. In mast cells these processes are triggered by antigen crosslinking of IgE bound to its high affinity receptor, FcεRI, on the cell surface. Here we use the endosomal v-SNARE, VAMP8, and the lysosomal hydrolase β-hexosaminidase (β-Hex), each C-terminally fused to super-ecliptic pHluorin, to monitor stimulated exocytosis. Using these pHluorin-tagged constructs, we monitor stimulated exocytosis by fluorimetry and visualize individual exocytic events with TIRF microscopy. Similar to constitutive recycling endosome (RE) trafficking, we find that stimulated RE exocytosis, monitored by VAMP8, is attenuated by expression of dominant negative (S25N) Rab11. Stimulated β-Hex exocytosis is also reduced in the presence of S25N Rab11, suggesting that expression of this mutant broadly impacts exocytosis. Interestingly, pretreatment with inhibitors of actin polymerization, cytochalasin D or latrunculin A, substantially restores both RE and lysosome exocytosis in cells expressing S25N Rab11. Conversely, stabilizing F-actin with jasplakinolide inhibits antigen-stimulated exocytosis but is not additive with S25N Rab11-mediated inhibition, suggesting that these reagents inhibit related processes. Together, our results suggest that Rab11 participates in the regulation necessary for depolymerization of the actin cytoskeleton during stimulated exocytosis in mast cells.

Keywords

Rab11; VAMP8; recycling endosome; exocytosis; degranulation; F-actin; TIRF

Introduction

Stimulated exocytosis events occur in numerous physiological processes, and they are a hallmark of the allergic immune response. Allergies and associated inflammatory processes are triggered by multivalent antigen (Ag)-mediated crosslinking of IgE bound to its high affinity Fc receptor, FcεRI, on the surface of mast cells and basophils. FcεRI aggregation initiates a signaling cascade that results in the release of chemical mediators via exocytosis of secretory lysosomes in the process commonly called degranulation (1). We previously reported that RBL-2H3 mast cells also undergo antigen-stimulated trafficking and exocytosis of REs labeled with cholera toxin B (2).

Corresponding author: Barbara Baird, 607-255-4095, fax: 607-255-4137, bab13@cornell.edu.

We have no conflict of interest to declare.

REs are an assembly of mildly acidic vesicles and tubules that return endocytosed components to the plasma membrane (PM) (3). REs are often concentrated proximal to the nucleus and Golgi apparatus (4) and represent an important reservoir of membrane that is delivered to the plasma membrane during stages of surface area expansion such as cell migration, phagocytosis, and synaptic remodeling (5-8). The role of RE exocytosis in the mast cell response to Ag remains undefined.

The small GTPase Rab11 is a central regulator of RE trafficking and is often used to define the RE membrane (4). Rab11 is found associated with perinuclear REs and has been implicated in endocytic recycling downstream of Rab5 (9-11). It is known to associate with a subunit of the exocyst-tethering complex, Sec15, (12) and more recently has been functionally implicated in the exocytosis of REs (13). Rab11 has a number of potential effector proteins, probably conferring multiple activities (14). Rab11 is among a large number of Rabs recently identified to influence Ag-stimulated mast cell exocytosis (15). However, a direct role for Rab11 in this process has not been delineated.

Here, we characterize Ag-stimulated exocytosis in RBL mast cells using fluorimetric assays and two-color TIRF microscopy imaging. Utilizing genetically encoded exocytic reporters, we find that Rab11 spatially and temporally correlates with sites of exocytosis. Expression of dominant negative (S25N) Rab11 inhibits stimulated exocytosis, which is rescued by drugs that interfere with actin polymerization. Stabilizing F-actin prior to Ag stimulation attenuates exocytosis but is not additive with S25N Rab11 inhibition, suggesting a functional relationship between Rab11 and actin dynamics. Antigen initiates rapid depolymerization of cortical actin, which correlates temporally with the initiation of exocytosis, consistent with the actin network posing a barrier to this process. Together, our data implicate Rab11 in mast cell exocytosis of both secretory lysosomes and REs, and they connect Rab11 activity to actin depolymerization, which releases the cytoskeleton's negative regulation of exocytosis when the mast cell is stimulated by Ag.

Results

Genetically encoded reporters of Ag-stimulated exocytosis

Previous studies from our laboratory and others have shown that, in addition to exocytosis of secretory lysosomes, mast cells undergo exocytosis of REs in response to antigen (2, 22, 23). To further characterize the endosomal exocytic response to antigen, we sought to develop an assay that would allow us to exploit genetically encoded inhibitors of endocytic recycling. Prior studies employed FITC-cholera toxin B or biotinylation to monitor exocytosis, but these are unsuitable for molecular genetic experiments on mast cells with low transfection efficiency such as the RBL-2H3 line (24). To overcome this limitation, we utilized super-ecliptic pHluorin, a variant of GFP with enhanced fluorescence quenching at acidic pH (25, 26). The pHluorin moiety is fused to the protein of interest such that it is located in the lumen of its resident compartment, and its fluorescence is quenched if the compartment is acidic. Upon exocytosis, the pHluorin moiety encounters the neutral pH of the extracellular medium and its fluorescence increases dramatically. Similar de-quenching of pHlourin fluorescence occurs for these constructs when cells are treated with ammonium chloride (NH_4Cl) or are fixed and permeabilized

We examined several candidate pHluorin-fusions to monitor stimulated endosomal exocytosis, including VAMP3-, VAMP8-, and transferrin receptor-pHluorin (TfnR-pHl). Confocal microscopy of fixed RBL cells expressing these constructs revealed a perinuclear pool coincident with mCherry-Rab11A (mCh-Rab11), which labels REs (Supplemental Figure S1). VAMP8 emerged as the most promising candidate because of its robust expression compared to TfnR-pHl (data not shown) and its low steady-state plasma membrane levels compared to VAMP3-pHl (Supplemental Figure S2). Endogenous VAMP8 has been reported to localize to secretory lysosomes and to be important for degranulation in mast cells (27-29). In other cell types, VAMP8 has been identified on endosomes positive for the Rab11 family of interacting proteins 3 (FIP3) (30, 31), as well as with VAMP2 and VAMP3 on cytoplasmic vesicles containing GLUT4 that are regulated by insulin (32). Consistent with its association with a recycling endosomal pool, our VAMP8-pHl construct partially localizes to a Rab11-positive perinuclear compartment as revealed in fixed and permeablilized cells (Figure 1A, Figure S1). There is also some degree of VAMP8-pHl coincidence with the lysosomal marker CD63 (Figure 1B) (33). To monitor secretory lysosome exocytosis more selectively, we made a construct consisting of the lysosomal protein β-hexosaminidase fused to pHluorin (β-Hex-pHl). In contrast to VAMP8-pHl, β-Hex-pHl does not concentrate with Rab11 (Figure 1A) but shows substantial overlap with CD63 (Figure 1B), consistent with lysosomal localization.

Exocytosis of transfected VAMP8-pHl or β-Hex-pHl can be monitored by steady-state fluorimetry. As shown in Figure 2A and B, fluorescence values are unchanged until the addition of Ag, which results in a gradual increase in signal over several minutes. VAMP8-pHl is a transmembrane protein and moves from endolysosomal membranes to the plasma membrane during exocytosis, whereas β-hex-pHl is soluble and is thus released into the extracellular medium upon degranulation. Ag stimulation of VAMP8-pHl expressing cells results in increasing pHluorin fluorescence starting from ~10-20 seconds after addition and reaching a steady-state after ~120-180 seconds (Figure 2A). The distribution of VAMP8-pHluorin before and after stimulation by antigen is shown in the TIRF images in Figure 3A (below). β-Hex-pHl shows a similar, albeit slower, increase in fluorescence (Figure 2B). Fluorescence values continue to rise with β-Hex-pHl throughout the time course measured (300 sec), whereas VAMP8-pHl values reach a plateau after ~150 sec (Figure 2A), possibly because exocytosis is balanced by endocytosis. Addition of NH_4Cl deacidifies intracellular luminal compartments (34), thus dequenching all pHluorin fluorescence and resulting in a total fluorescence value that we use for normalization purposes (described in Materials and Methods). Following an initial increase in fluorescence due to endosomal de-acidification, we observed a decline in fluorescence following NH_4Cl addition that appears to be due to re-acidification, as it is sensitive to the vacuolar (lysosomal)-ATPase inhibitor bafilomycin A1 (Figure 2C), consistent with pHluorin quenching due to re-acidification of luminal compartments.

Rab11 marks sites of VAMP8-pHluorin exocytosis

Rab11 is known to be important for constitutive trafficking involving the RE (reviewed in 4) and has recently been shown by TIRF microscopy to be present on transferrin-labeled vesicles as they exocytose (13). Visualization of cortical/PM-proximal mCh-Rab11 by TIRF

microscopy reveals a dynamic cytoplasmic pool that is dispersed at the PM upon Ag stimulation (Figure 3A and Movie 1). This dispersion tends to start at the perimeter of the cell and move towards the center, suggesting that exocytosis may be triggered by localized FcεRI signaling along the path of Ag diffusion and receptor engagement on the ventral side of adherent cell as visualized with TIRF (35). This two-color TIRF microscopy experiment also demonstrates the dramatic exocytosis of VAMP8-pHl, resulting a significant fluorescence increase at the plasma membrane (Figures 3A and 6A; Movies 1 and 3). Closer examination of these recordings reveals that roughly two-thirds VAMP8-pHluorin exocytic events (376 of 508, Movie 2) appeared to be contributed by membrane co-labeled with mCherry-Rab11. We found that mCh-Rab11 most often disperses after the exocytic event, implying that it is on the endosomal membrane that undergoes the fusion event (Figure 3B, quantified in Figure 3C). Less frequently, mCh-Rab11-labeled puncta remained intact after an initial VAMP8-pHl fusion event, suggesting a larger mCh-Rab11-labeled membrane compartment donates VAMP8-pHl-containing vesicles that then fuse with the PM (Movie 3).

A similar examination of β-Hex-pHl and mCh-Rab11 showed that Rab11 does not associate with large, degranulation-type exocytic events labeled by β-Hex-pHl. However, a small amount of β-Hex-pHl releases coincident with some mCh-Rab11 exocytosis events (Movie 4). This most likely represents a small amount of β-Hex-pHl being mis-sorted to REs, but could also indicate a role for Rab11 in the exocytosis of a subset of degranulation events. These data provide direct evidence for Rab11 participation in the exocytic response to Ag. Furthermore, they support the utility of VAMP8-pHl as a reporter of Ag-stimulated RE exocytosis.

Dominant negative Rab11 (S25N) inhibits Ag-stimulated exocytosis

Because most VAMP8-pHl vesicles undergoing Ag-stimulated exocytosis are also labeled with mCh-Rab11, we reasoned that Rab11 might have an active role in regulating this process. Dominant negative (S25N) Rab11 has been shown to interfere with constitutive RE pathways (9, 11, 13), and we asked if it would affect stimulated VAMP8-pHl exocytosis. VAMP8-pHl was co-expressed with either wild-type (WT) or S25N mCh-Rab11, and Ag-stimulated VAMP8-pHl exocytosis was monitored by fluorimetry. As shown in Figure 4A, expression of S25N Rab11 reduces Ag-stimulated VAMP8-pHl exocytosis to approximately one third the level of cells co-expressing WT Rab11. We observed a similar trend when we examined the effect of S25N Rab11 on antigen-stimulated exocytosis of the RE resident protein TfnR-pHl (J.D. Wilson, unpublished results).

Interestingly, pretreatment with the actin polymerization inhibitor cytochalasin D (cyto D) rescues S25N Rab11-inhibited VAMP8-pHl exocytosis to approximately two thirds of the response in cells expressing WT Rab11 (Figure 4A bar graph). VAMP8-pHl exocytosis in the presence of WT Rab11 is also enhanced by cyto D pretreatment, but to a smaller extent (~1.3 fold for WT +/− cyto D versus ~2.8 fold for S25N +/− cyto D). We observed a similar rescue of inhibition by S25N Rab11 with latrunculin A (lat A) (Figure S3), indicating that this result is due to inhibition of actin polymerization.

Drugs that inhibit actin polymerization, including cyto D and latrunculin B, are known to enhance degranulation in mast cells (36, 37). Furthermore, these drugs increase Ag-stimulated tyrosine phosphorylation (37, 38), suggesting a possible explanation for the elevated degranulation. To test if enhanced upstream signaling accounts for the cyto D-mediated rescue of S25N Rab11 inhibition, we bypassed FcεRI signaling by stimulating exocytosis with the Ca^{2+} ionophore A23187 (A23) (39). As shown in Figure 4B, S25N Rab11 inhibits A23-stimulated VAMP8-pHl exocytosis to ~45% of WT Rab11 levels. Similar to the results with Ag, S25N Rab11 inhibition is partially rescued by cyto D (Figure 4B bar graph), indicating that enhanced early FcεRI signaling is not the primary explanation for the rescue.

We tested whether S25N Rab11, which inhibits RE exocytosis, also affects degranulation. We co-expressed β-Hex-pHl with WT or S25N mCh-Rab11 and monitored Ag-stimulated exocytosis by fluorimetry. Interestingly, β-Hex-pHl exocytosis is also inhibited by S25N Rab11 (Figure 4C). Similar to the results with VAMP8-pHl, cyto D pretreatment also substantially rescues S25N Rab11 inhibition of β-Hex-pHl exocytosis (Figure 4C, bar graph). Thus, inhibition of actin polymerization functionally reduces the Rab11 requirement during stimulated exocytosis. Furthermore, these results point to a connection between Rab11 activity and release of F-actin's suppression of exocytosis when cells are stimulated by Ag.

Jasplakinolide inhibits stimulated VAMP8-pHl exocytosis

The results described above are consistent with the hypothesis that cortical F-actin acts as a physical barrier to exocytosis in the absence of stimulation (reviewed in 40). It was previously shown that jasplakinolide (jasp), which stabilizes F-actin (41-43), has an inhibitory effect on degranulation in bone marrow-derived mast cells and RBL cells (44, 45). We tested whether jasp also inhibits Ag-stimulated exocytosis monitored in cells co-expressing VAMP8-pHl and either WT or S25N Rab11. Indeed, as shown in Figure 5A, Ag-stimulated exocytosis in cells expressing WT Rab11 is significantly inhibited by jasp pretreatment. Interestingly, jasp has a minimal additive effect on stimulated exocytosis attenuated by S25N Rab11.

To test whether jasp mediates this inhibition by interfering with early FcεRI signaling events, we monitored A23-stimulated VAMP8-pHl exocytosis in the context of WT or S25N Rab11 and observed a similar level of jasp-mediated inhibition (Figure 5B). Similar to Ag-stimulated cells, jasp inhibition is not additive with S25N Rab11-mediated inhibition, suggesting that S25N Rab11 expression maximally inhibits Ag-stimulated actin depolymerization process that jasp also prevents. Together with the capacity of cyto D and lat A to overcome the effects of S25N Rab11, these results support the hypothesis that F-actin forms a physical barrier to exocytosis that is reversed during Ag stimulation as regulated by Rab11.

Ag-stimulated exocytosis is temporally correlated with cortical actin dynamics

Actin dynamics are known to be driven by Ag stimulation (37, 45-47). F-actin levels have been reported to drop soon after Ag addition and then climb to levels above those found in

resting cells within ~1 minute post-Ag addition (46). Using two-color TIRF microscopy, we simultaneously monitored Ag-stimulated exocytosis with VAMP8-pHl and cortical F-actin labeled with LifeAct-mApple (Figure 6A and Movie 5). Consistent with previous reports, we observe a decrease in cortical F-actin levels soon after Ag addition. A minimum value was reached approximately 30 seconds post-Ag addition, and cortical F-actin subsequently returned as dynamic puncta, with appearance of actin filaments at later time points. We observed that the onset of the rise in VAMP8-pHl fluorescence (via exocytosis) temporally correlates with the minimum for polymerized actin (Figure 6B), suggesting that this decrease in cortical F-actin is required for exocytosis. Together with our data showing that cyto D and lat A reduce S25N Rab11 inhibition of Ag stimulated exocytosis, this result is consistent with S25N Rab11 interfering with an Ag-stimulated decrease in cortical F-actin, thereby inhibiting exocytosis.

We tested and did not detect with LifeAct-mApple and TIRF microscopy a reproducible influence of S25N Rab11 on Ag-stimulated F-actin dynamics, although these are affected by both lat A and cyto D (data not shown). It is likely that more subtle effects of S25N Rab11 on F-actin levels are swamped out by other stimulated actin activities reported by the LifeAct probe.

Interestingly, we observed that a considerable fraction of the LifeAct-labeled puncta appearing in the TIRF field after Ag stimulation are recruited to regions of the plasma membrane that are devoid of VAMP8-pHl fluorescence (Figure 6A,C). Other experiments showed that these regions also excluded a cytosolic label (data not shown), suggesting that they may be invaginations in the plasma membrane. Furthermore, some of these apparent invaginations correlate with sites of β-Hex-pHl exocytosis (data not shown). Thus, it appears that a subset of the cortical actin dynamics observed in Ag-stimulated cells involves the recruitment of F-actin to regions that have recently undergone exocytosis of secretory lysosomes. The observed recruitment of actin puncta is often followed by their disappearance and a return of VAMP8-pHl to the plasma membrane in the same regions (Figure 6C far right image), suggesting that actin is involved in localized remodeling of the plasma membrane. Previous studies in RBL cells detected the appearance of actin plaques at the plasma membrane as a consequence of Ag stimulation (48), and the location of these may possibly correspond to sites of exocytosis.

p50RhoGAP links Rab11 to F-actin dynamics

We investigated the mechanistic relationship between Rab11 activity and F-actin dynamics during stimulated exocytosis. p50RhoGAP, a Rho GTPase activating protein also known as Cdc42GAP or ArhGAP1, has been reported to interact with WT Rab11 and to localize to Rab5- and Rab11-labeled endosomal compartments in HeLa cells (20). In another study, p50RhoGAP was identified on Rab11-FIP3 endosomes and implicated in regulating F-actin during cytokinesis (30). Consistent with these published results, we found that a significant fraction of p50RhoGAP-GFP coincides with WT mCh-Rab11 in RBL cells (Figure S4A). In contrast, p50RhoGAP-GFP shows less co-localization with S25N mCh-Rab11 (Figure S4B), which concentrates at the trans-Golgi network (49)

Sirokmany et al. reported that expression of the N-terminal Sec14 homology domain (NTD) of p50RhoGAP inhibits transferrin uptake and recycling (20). The mechanism of this inhibition is unknown. Thus, we tested whether expression of NTD disrupts F-actin depolymerization during Ag stimulation, which we would expect to inhibit exocytosis. To focus on the exocytic process, we co-expressed β-Hex-pHl together with either full-length (FL) p50RhoGAP or NTD and monitored Ag-stimulated β-Hex-pHl exocytosis by fluorimetry. As shown in Figure 7, expression of NTD attenuates β-Hex-pHl exocytosis compared with cells expressing FL p50RhoGAP. This inhibition is partially rescued by cyto D, indicating that, similar to the restoration of exocytosis inhibited by S25N Rab11, inhibition of actin polymerization during Ag stimulation reduces the requirement for p50RhoGAP. Thus it appears that Rab11 is activated by p50RhoGAP to facilitate actin depolymerization during Ag-stimulated exocytosis.

Discussion

Physiological signaling often involves cellular exocytosis of cytoplasmic vesicles to remodel the plasma membrane or to release chemical mediators. A prominent example is mast cells, which respond to antigenic stimuli with a burst of exocytosis of both secretory lysosomes, containing mediators of inflammation and allergy, and REs (2,22). Our examination of Ag-stimulated exocytosis in RBL mast cells with genetically encoded exocytic reporters led to a new level of characterization including strong evidence that Rab11 plays a key regulatory role. We found that Rab11 is present on exocytic vesicles corresponding to REs and much less on secretory lysosomes (Figure 1). Interestingly, dominant negative (S25N) Rab11 inhibits exocytosis of both types. This inhibition is relieved by pre-incubation with the inhibitors of actin polymerization, cyto D and lat A (Figures 4 and S3). Jasp, which stabilizes F-actin, inhibits VAMP8-mediated exocytosis (Figure 5), similar to the effect of S25N Rab11. Together, these results indicate that Rab11 regulates the dynamics of F-actin depolymerization during the exocytic response to Ag. Consistent with this hypothesis, a dominant negative mutant of the actin regulatory protein p50RhoGAP also inhibits exocytosis of secretory lysosomes (Figure 7).

Rab11 participates in stimulated exocytosis downstream of early signaling as indicated by S25N Rab11 inhibiting exocytosis of VAMP8-pHI that is stimulated by the Ca^{2+} ionophore A23 (Figure 4), which by-passes early signaling events. Furthermore, the restoration of exocytosis by cyto D and lat A suggests that S25N Rab11 interferes with a change in the actin polymerization state required for effective vesicle fusion with the plasma membrane. Previous studies suggest Rab11 is involved in the docking of RE-derived vesicles at the plasma membrane (13). Others have reported that constitutively active Rab11, compared to other Rab proteins, interferes with secretory lysosome exocytosis in RBL-2H3 cells, suggesting that GDP/GTP cycling of Rab11 is involved (15). Azouz et al. also found that, similar to our results with S25N Rab11, the inhibitory effect of constitutively active Rab11 is relieved by treatment with cyto D (15). We have confirmed the inhibitory effect of constitutively active Rab11, which is smaller than that of S25N Rab11, but is consistent with a role for GDP/GTP cycling of this Rab protein in stimulated exocytosis.

Rab11 has little, if any, steady-state presence on lysosomes (Figure 1 and ref.15), consistent with the view that the effect of S25N Rab11 on degranulation occurs through regulation of actin dynamics at the plasma membrane. It is likely that Rho GTPases and associated proteins are recruited to the cortical cytoskeleton to regulate the actin meshwork during Ag-mediated signaling (45, 47). Rab11 may modulate Rho activity and the actin meshwork through association with proteins such as p50RhoGAP (20, 30).

Drugs that interfere with actin polymerization are known to enhance degranulation in RBL mast cells (36, 37). The mechanism probably includes a combination of enhancement of early signaling events (FcεRI phosphorylation) and reduction of cortical F-actin that physically impedes exocytosis (37, 38, 45). Expression of S25N Rab11 in maturing oocytes has been shown to dramatically stabilize the actin network (50), consistent with F-actin forming an exocytic barrier in RBL cells under conditions of S25N Rab11 or NTD-p50RhoGAP expression. We did not detect gross alternations in cortical F-actin structure or dynamics in cells expressing these constructs (data not shown), which suggests that their effects are localized and subtle compared to the overall cytoskeletal activity upon Ag stimulation. The dynamic remodeling of cortical F-actin we observe, and its relative disappearance in the TIRF field following Ag stimulation correlates with the initiation of exocytosis (Figure 6). However, the general LifeAct label and TIRF microscopy are not sufficiently sensitive to discern the F-actin remodeling important for efficient exocytosis that we characterize with selective exocytic vesicle reporters.

The basis for net trafficking of REs to the plasma membrane in mast cells during Ag stimulation remains to be determined. We did not detect a similar RE exocytic response using Ca^{2+} ionophore in HeLa or N2A cells (data not shown), suggesting that mast cell REs may possess specialized machinery, such as particular synaptotagmins, that sensitize this population of intracellular vesicles to Ca^{2+}-based signaling. REs likely represent important membrane stores for plasma membrane expansion (5-7). Furthermore, the targeting of RE membrane to sites of FcεRI aggregation (22) may be necessary for spatially directed delivery of components involved in the cell's response to Ag, including stimulated internalization of IgE-FcεRI crosslinked by Ag. Interestingly, it was recently reported that cytotoxic T lymphocytes use recycling endosomes to deliver syntaxin-11, a SNARE important for cytotoxic granule exocytosis (51). Further characterization of the participating machinery will serve to reveal the structural basis and the functional consequences of RE exocytosis in mast cells during Ag stimulation.

Materials and Methods

Reagents

Preparation of mouse monoclonal anti-DNP IgE antibody (16) and DNP-BSA (Ag) (17) have been described. A23187 was from EMD Millipore. Jasplakinolide and latrunculin A were from Life Technologies. Mouse monoclonal anti-CD63 (clone AD1, BD Pharmingen), rabbit monoclonal anti-Rab11 (clone D4F5, Cell Signaling), Alexa Fluor 568 goat anti-rabbit (H+L), and Alexa Fluor 647-conjugated goat anti-mouse IgG_1 antibodies (Life Technologies/Molecular Probes) are available commercially. Other reagents were acquired from Sigma-Aldrich Chem. Co. or Fisher Scientific, Inc., except where noted.

Plasmids

LifeAct-mApple was a gift from M. Korzeniowski (Cornell University, Ithaca, NY). Super-ecliptic pHluorin (26), as a fusion with transferrin receptor (human) in the vector jPA5 (18), was a gift from P. De Camilli (Yale University, New Haven, CT). To create the pHluorin-fusion constructs, the transferrin receptor fragment was removed from the jPA5 construct using *Eco*RI and *Age*I sites and replaced with cDNA encoding VAMP3 (rat, gift from S. Grinstein, U. Toronto), VAMP8 (mouse, Open Biosystems), or β-Hexosamindase A (rat, Open Biosystems). VAMP8-mNectarine was constructed by replacing pHluorin in the VAMP8 jPA5 construct with mNectarine (19) (Addgene plasmid ID # 21717) using *Age*I and *Hin*dIII sites. To make mCherry-Rab11, EGFP in EGFP-C1 (Clontech) was replaced with mCherry using *Nhe*I and *Hin*dIII sites. Rab11A cDNA (human, from R. Collins, Cornell University, Ithaca, NY) was then subcloned using *Eco*RI and *Bam*HI sites. The S25N mutation was introduced using site-directed mutagenesis. p50RhoGAP (human, Open Biosystems), full length or an N-terminal domain (NTD) fragment encoding the Sec14-like domain (amino acids 1-222) (20), was subcloned into EGFP-N1 (Clontech) using *Xho*I and *Eco*RI sites. The mCherry variants of these constructs were made by replacing EGFP with mCherry using *Age*I and *Not*I sites. Molecular biology reagents were purchased from New England Biolabs.

Cell Culture and transfection

RBL-2H3 cells (21) were grown at 37°C and 5% CO_2 in RBL medium consisting of Minimal Essential Medium with Earle's salts (Invitrogen), 20% fetal bovine serum (Atlanta Biologicals), and 10 μg/ml gentamicin sulfate (Life Technologies). For transfections, cells were incubated at 37°C in Opti-MEM I (Life Technologies) with FuGENE HD (Promega) DNA complexes 3 μg/ml DNA (for cotransfections: ~3:1 dominant negative (or WT) to reporter; equal ratio for microscopy) and 8 μl/ml FuGENE HD for ~1.5 hours, at which time 0.1 μM phorbol 12,13-dibutyrate (PDB) was added to for an additional ~3.5 hours. PDB was removed by washing, and cells were incubated in RBL medium overnight to allow expression of transfected gene(s).

Fluorimetry

Approximately 2.5 million RBL-2H3 cells per condition were plated in 60 mm dishes, transfected on two consecutive days, and sensitized for 16-24 hours prior to the experiment with 0.5-1 μg/ml anti-DNP IgE. Cells were then harvested, washed, and resuspended in buffered saline solution (BSS: 20 mM HEPES-NaOH, 135 mM NaCl, 5 mM KCl, 1.8 mM $CaCl_2$, 1 mM $MgCl_2$, 5.6 mM D-glucose, pH 7.5) with 1 mg/ml bovine serum albumin. Cells were placed in a 10 × 10 × 40 mm acrylic cuvette at ~1-2 × 10^6 cells/ml in BSS and pre-equilibrated at 37°C for 5 minutes with continuous stirring. pHluorin fluorescence (ex. 470 nm, em. 508 nm) was monitored using a SLM 8100C steady-state fluorescence spectrophotometer in ratio mode (SLM Instruments). After stimulation with Ag (100 ng/ml DNP-BSA) or calcium ionophore A23187 (1 μM), total fluorescence values were obtained by adding 50 mM NH_4Cl to equilibrate endosomal contents with the extracellular pH. Samples to be compared were first adjusted by subtracting baseline fluorescence (t=0) from each subsequent fluorescence value. For plots presented in Figures 4, 5, 7, and Supplemental

Figure S3, baseline-subtracted data were normalized to the baseline-subtracted total fluorescence value obtained at the peak following NH_4Cl addition. GraphPad software was used to compute p-values (unpaired *t*-test).

Microscopy

For all microscopy experiments, 1-3 × 10^5 cells were plated in 35 mm glass bottom dishes (MatTek Corp.), transfected on day 2, and imaged or fixed on day 3. For confocal microscopy, cells were washed with 37°C phosphate buffered saline (PBS) and then fixed with 37°C 4% paraformaldehyde (Electron Microscopy Sciences) and 0.1% glutaraldehyde in PBS at room temperature for 10-15 minutes. The fixing reaction was quenched using PBS, pH 7.4, with 1% BSA and 0.05% NaN_3 (blocking buffer). For immunofluorescence experiments, cells were incubated with specific antibodies (3 hours, diluted 1:100 for anti-Rab11 (clone D4F5, Cell Signaling Technologies) and 1 hour, 50 μg/ml for anti-CD63 (clone AD1, BD Pharmingen)) in blocking buffer supplemented with 0.1% Triton X-100 and 0.25 mg/ml non-specific human IgG, washed with blocking buffer, and incubated for 1 hour at room temperature with secondary antibodies diluted to 10 μg/ml in blocking buffer. After washing with blocking buffer, cells were stored and imaged in PBS with 1% BSA. Confocal microscopy was performed with a Zeiss LSM710 microscope (Biotechnology Resource Center, Cornell University, Ithaca, NY), using a Plan-APOCHROMAT 63X, 1.4 NA oil immersion objective.

Live cell TIRF movies were acquired on an inverted microscope (Leica DM-IRB, Wetzlar, Germany) under illumination through a 1.42 NA 100X Leica TIRF objective lens. Samples were kept at approximately 34°C during imaging using an objective heater (Bioptechs, Butler, PA) coupled to the TIRF objective. 100W 488 and 561 nm diode-pumped solid state lasers (Coherent, Santa Clara, CA), attenuated with neutral density filters as needed to prevent sample photobleaching and phototoxicity, were used for TIRF illumination. Multi-bandpass excitation, polychromic, and emission filters (Chroma Technology Inc., Burlington, VT) were used to simultaneously admit illumination from 488 and 561 nm lasers and pass emission from both channels. The two color channels were further separated onto two distinct regions of the camera CCD using an Optosplit emission splitter (Cairn, Faversham, UK). Images were recorded with an Andor iXon 897 EM-CCD camera (Andor, Belfast, UK) using proprietary Andor software as well as custom image acquisition code written in Matlab (The MathWorks, Natick, MA). Movies of live cells were acquired in 1000-frame increments. A 0.15 sec camera exposure time (5.4 fps frame rate) was used for live cell movie acquisition throughout, with variable EM-CCD gain settings and illumination intensity depending on the signal-to-noise of the fluorescence signal. Ag in BSS was added at 200 ng/ml. Focus was manually adjusted.

TIRF images were analyzed and converted to AVI files using ImageJ/Fiji (NIH, Bethesda, MD). Exocytic events were counted manually, sometimes with the Cell Counter plugin. The Z Profiler plugin was used to quantify regions of interest signal intensity, and data were normalized between 0 and 1. The Series Labeler plugin was used to add time stamps to movies. For mCh-Rab11 coincidence with VAMP8-pHl exocytosis, Rab11 involvement was scored positive if an exocytic event coincided with Rab11 signal and resulted in subsequent

Rab11 dispersion or rapid movement away from site of exocytosis. VAMP8-pHl exocytosis simply occurring proximal to or overlapping with a pool of mCh-Rab11 was not considered positive for Rab11 involvement.

Supplementary Material

Refer to Web version on PubMed Central for supplementary material.

Acknowledgements

We thank Drs. Ruth Collins, Pietro de Camilli, Sergio Grinstein, and Marek Korzeniowski for DNA constructs. We also thank Drs. Norah Smith and Roy Cohen for helpful advice, and Dr. Alice Wagenknecht-Wiesner and Ms. Hayley Knox for technical assistance. We acknowledge Carol Bayles of the Cornell University Biotechnology Resource Center for assistance with the Zeiss LSM 710 Confocal microscope funded by NIH 1S10RR025502-01. This work was supported by NIH NRSA Fellowship F32GM095183 to JDW and by the National Institute of Allergy and Infectious Diseases Grant R01AI022449.

References

1. Blank U, Rivera J. The ins and outs of IgE-dependent mast-cell exocytosis. Trends Immunol. 2004; 25(5):266–273. [PubMed: 15099567]
2. Naal RM, Holowka EP, Baird B, Holowka D. Antigen-stimulated trafficking from the recycling compartment to the plasma membrane in RBL mast cells. Traffic. 2003; 4(3):190–200. [PubMed: 12656991]
3. Yamashiro DJ, Tycko B, Fluss SR, Maxfield FR. Segregation of transferrin to a mildly acidic (pH 6.5) para-Golgi compartment in the recycling pathway. Cell. 1984; 37(3):789–800. [PubMed: 6204769]
4. Grant BD, Donaldson JG. Pathways and mechanisms of endocytic recycling. Nat Rev Mol Cell Biol. 2009; 10(9):597–608. [PubMed: 19696797]
5. Cox D, Lee DJ, Dale BM, Calafat J, Greenberg S. A Rab11-containing rapidly recycling compartment in macrophages that promotes phagocytosis. Proc Natl Acad Sci U S A. 2000; 97(2): 680–685. [PubMed: 10639139]
6. Bajno L, Peng XR, Schreiber AD, Moore HP, Trimble WS, Grinstein S. Focal exocytosis of VAMP3-containing vesicles at sites of phagosome formation. J Cell Biol. 2000; 149(3):697–706. [PubMed: 10791982]
7. Park M, Salgado JM, Ostroff L, Helton TD, Robinson CG, Harris KM, Ehlers MD. Plasticity-induced growth of dendritic spines by exocytic trafficking from recycling endosomes. Neuron. 2006; 52(5):817–830. [PubMed: 17145503]
8. Bretscher MS, Aguado-Velasco C. EGF induces recycling membrane to form ruffles. Curr Biol. 1998; 8(12):721–724. [PubMed: 9637926]
9. Ullrich O, Reinsch S, Urbe S, Zerial M, Parton RG. Rab11 regulates recycling through the pericentriolar recycling endosome. J Cell Biol. 1996; 135(4):913–924. [PubMed: 8922376]
10. Sonnichsen B, De Renzis S, Nielsen E, Rietdorf J, Zerial M. Distinct membrane domains on endosomes in the recycling pathway visualized by multicolor imaging of Rab4, Rab5, and Rab11. J Cell Biol. 2000; 149(4):901–914. [PubMed: 10811830]
11. Ren M, Xu G, Zeng J, De Lemos-Chiarandini C, Adesnik M, Sabatini DD. Hydrolysis of GTP on rab11 is required for the direct delivery of transferrin from the pericentriolar recycling compartment to the cell surface but not from sorting endosomes. Proc Natl Acad Sci U S A. 1998; 95(11):6187–6192. [PubMed: 9600939]
12. Zhang XM, Ellis S, Sriratana A, Mitchell CA, Rowe T. Sec15 is an effector for the Rab11 GTPase in mammalian cells. J Biol Chem. 2004; 279(41):43027–43034. [PubMed: 15292201]
13. Takahashi S, Kubo K, Waguri S, Yabashi A, Shin HW, Katoh Y, Nakayama K. Rab11 regulates exocytosis of recycling vesicles at the plasma membrane. J Cell Sci. 2012; 125:4049–4057. Pt 17. [PubMed: 22685325]

14. Horgan CP, McCaffrey MW. The dynamic Rab11-FIPs. Biochem Soc Trans. 2009; 37:1032–1036. Pt 5. [PubMed: 19754446]
15. Azouz NP, Matsui T, Fukuda M, Sagi-Eisenberg R. Decoding the regulation of mast cell exocytosis by networks of Rab GTPases. J Immunol. 2012; 189(5):2169–2180. [PubMed: 22826321]
16. Posner RG, Lee B, Conrad DH, Holowka D, Baird B, Goldstein B. Aggregation of IgE-receptor complexes on rat basophilic leukemia cells does not change the intrinsic affinity but can alter the kinetics of the ligand-IgE interaction. Biochemistry. 1992; 31(23):5350–5356. [PubMed: 1534998]
17. Weetall M, Holowka D, Baird B. Heterologous desensitization of the high affinity receptor for IgE (Fc epsilon R1) on RBL cells. J Immunol. 1993; 150(9):4072–4083. [PubMed: 8473750]
18. Merrifield CJ, Perrais D, Zenisek D. Coupling between clathrin-coated-pit invagination, cortactin recruitment, and membrane scission observed in live cells. Cell. 2005; 121(4):593–606. [PubMed: 15907472]
19. Johnson DE, Ai HW, Wong P, Young JD, Campbell RE, Casey JR. Red fluorescent protein pH biosensor to detect concentrative nucleoside transport. J Biol Chem. 2009; 284(31):20499–20511. [PubMed: 19494110]
20. Sirokmany G, Szidonya L, Kaldi K, Gaborik Z, Ligeti E, Geiszt M. Sec14 homology domain targets p50RhoGAP to endosomes and provides a link between Rab and Rho GTPases. J Biol Chem. 2006; 281(9):6096–6105. [PubMed: 16380373]
21. Barsumian EL, Isersky C, Petrino MG, Siraganian RP. IgE-induced histamine release from rat basophilic leukemia cell lines: isolation of releasing and nonreleasing clones. Eur J Immunol. 1981; 11(4):317–323. [PubMed: 6166481]
22. Wu M, Baumgart T, Hammond S, Holowka D, Baird B. Differential targeting of secretory lysosomes and recycling endosomes in mast cells revealed by patterned antigen arrays. J Cell Sci. 2007; 120:3147–3154. Pt 17. [PubMed: 17698921]
23. Liao H, Keller SR, Castle JD. Insulin-Regulated Aminopeptidase Marks an Antigen-Stimulated Recycling Compartment in Mast Cells. Traffic. 2006; 7(2):155–167. [PubMed: 16420524]
24. Gosse JA, Wagenknecht-Wiesner A, Holowka D, Baird B. Transmembrane sequences are determinants of immunoreceptor signaling. J Immunol. 2005; 175(4):2123–2131. [PubMed: 16081778]
25. Sankaranarayanan S, De Angelis D, Rothman JE, Ryan TA. The use of pHluorins for optical measurements of presynaptic activity. Biophys J. 2000; 79(4):2199–2208. [PubMed: 11023924]
26. Miesenbock G, De Angelis DA, Rothman JE. Visualizing secretion and synaptic transmission with pH-sensitive green fluorescent proteins. Nature. 1998; 394(6689):192–195. [PubMed: 9671304]
27. Puri N, Roche PA. Mast cells possess distinct secretory granule subsets whose exocytosis is regulated by different SNARE isoforms. Proc Natl Acad Sci U S A. 2008; 105(7):2580–2585. [PubMed: 18250339]
28. Tiwari N, Wang C-C, Brochetta C, Ke G, Vita F, Qi Z, Rivera J, Soranzo MR, Zabucchi G, Hong W, Blank U. VAMP-8 segregates mast cell-preformed mediator exocytosis from cytokine trafficking pathways. Blood. 2008; 111(7):3665–3674. [PubMed: 18203950]
29. Paumet F, Le Mao J, Martin S, Galli T, David B, Blank U, Roa M. Soluble NSF Attachment Protein Receptors (SNAREs) in RBL-2H3 Mast Cells: Functional Role of Syntaxin 4 in Exocytosis and Identification of a Vesicle-Associated Membrane Protein 8-Containing Secretory Compartment. J Immunol. 2000; 164(11):5850–5857. [PubMed: 10820264]
30. Schiel JA, Simon GC, Zaharris C, Weisz J, Castle D, Wu CC, Prekeris R. FIP3-endosome-dependent formation of the secondary ingression mediates ESCRT-III recruitment during cytokinesis. Nat Cell Biol. 2012; 14(10):1068–1078. [PubMed: 23000966]
31. Schiel JA, Park K, Morphew MK, Reid E, Hoenger A, Prekeris R. Endocytic membrane fusion and buckling-induced microtubule severing mediate cell abscission. J Cell Sci. 2011; 124:1411–1424. Pt 9. [PubMed: 21486954]
32. Zhao P, Yang L, Lopez JA, Fan J, Burchfield JG, Bai L, Hong W, Xu T, James DE. Variations in the requirement for v-SNAREs in GLUT4 trafficking in adipocytes. J Cell Sci. 2009; 122:3472–3480. Pt 19. [PubMed: 19759285]

33. Nishikata H, Oliver C, Mergenhagen SE, Siraganian RP. The rat mast cell antigen AD1 (homologue to human CD63 or melanoma antigen ME491) is expressed in other cells in culture. J Immunol. 1992; 149(3):862–870. [PubMed: 1634775]
34. Poole B, Ohkuma S. Effect of weak bases on the intralysosomal pH in mouse peritoneal macrophages. J Cell Biol. 1981; 90(3):665–669. [PubMed: 6169733]
35. Shelby SA, Holowka D, Baird B, Veatch SL. Distinct stages of stimulated FcepsilonRI receptor clustering and immobilization are identified through superresolution imaging. Biophys J. 2013; 105(10):2343–2354. [PubMed: 24268146]
36. Narasimhan V, Holowka D, Baird B. Microfilaments regulate the rate of exocytosis in rat basophilic leukemia cells. Biochem Biophys Res Commun. 1990; 171(1):222–229. [PubMed: 2203345]
37. Frigeri L, Apgar JR. The role of actin microfilaments in the down-regulation of the degranulation response in RBL-2H3 mast cells. J Immunol. 1999; 162(4):2243–2250. [PubMed: 9973500]
38. Holowka D, Sheets ED, Baird B. Interactions between Fc(epsilon)RI and lipid raft components are regulated by the actin cytoskeleton. J Cell Sci. 2000; 113:1009–1019. Pt 6. [PubMed: 10683149]
39. Reed PW, Lardy HA. A23187: a divalent cation ionophore. J Biol Chem. 1972; 247(21):6970–6977. [PubMed: 4263618]
40. Nightingale TD, Cutler DF, Cramer LP. Actin coats and rings promote regulated exocytosis. Trends Cell Biol. 2012; 22(6):329–337. [PubMed: 22543050]
41. Crews P, Manes LV, Boehler M. Jasplakinolide, a cyclodepsipeptide from the marine sponge, Jaspis SP. Tetrahedron Letters. 1986; 27(25):2797–2800.
42. Bubb MR, Senderowicz AM, Sausville EA, Duncan KL, Korn ED. Jasplakinolide, a cytotoxic natural product, induces actin polymerization and competitively inhibits the binding of phalloidin to F-actin. J Biol Chem. 1994; 269(21):14869–14871. [PubMed: 8195116]
43. Bubb MR, Spector I, Beyer BB, Fosen KM. Effects of jasplakinolide on the kinetics of actin polymerization. An explanation for certain in vivo observations. J Biol Chem. 2000; 275(7):5163–5170. [PubMed: 10671562]
44. Nishida K, Yamasaki S, Ito Y, Kabu K, Hattori K, Tezuka T, Nishizumi H, Kitamura D, Goitsuka R, Geha RS, Yamamoto T, Yagi T, Hirano T. Fc{epsilon}RI-mediated mast cell degranulation requires calcium-independent microtubule-dependent translocation of granules to the plasma membrane. J Cell Biol. 2005; 170(1):115–126. [PubMed: 15998803]
45. Wollman R, Meyer T. Coordinated oscillations in cortical actin and Ca2+ correlate with cycles of vesicle secretion. Nat Cell Biol. 2012; 14(12):1261–1269. [PubMed: 23143397]
46. Pfeiffer JR, Seagrave JC, Davis BH, Deanin GG, Oliver JM. Membrane and cytoskeletal changes associated with IgE-mediated serotonin release from rat basophilic leukemia cells. J Cell Biol. 1985; 101(6):2145–2155. [PubMed: 2933414]
47. Wu M, Wu X, De Camilli P. Calcium oscillations-coupled conversion of actin travelling waves to standing oscillations. Proc Natl Acad Sci U S A. 2013; 110(4):1339–1344. [PubMed: 23297209]
48. Pfeiffer JR, Oliver JM. Tyrosine kinase-dependent assembly of actin plaques linking Fc epsilon R1 cross-linking to increased cell substrate adhesion in RBL-2H3 tumor mast cells. J Immunol. 1994; 152(1):270–279. [PubMed: 7504712]
49. Chen W, Feng Y, Chen D, Wandinger-Ness A. Rab11 is required for trans-golgi network-to-plasma membrane transport and a preferential target for GDP dissociation inhibitor. Mol Biol Cell. 1998; 9(11):3241–3257. [PubMed: 9802909]
50. Holubcova Z, Howard G, Schuh M. Vesicles modulate an actin network for asymmetric spindle positioning. Nat Cell Biol. 2013; 15(8):937–947. [PubMed: 23873150]
51. Marshall MR, Pattu V, Halimani M, Maier-Peuschel M, Müller M-L, Becherer U, Hong W, Hoth M, Tschernig T, Bryceson YT, Rettig J. VAMP8-dependent fusion of recycling endosomes with the plasma membrane facilitates T lymphocyte cytotoxicity. The Journal of Cell Biology. 2015; 210(1):135–151. [PubMed: 26124288]

Synopsis

Mast cell exocytosis causes allergy through the release of mediators from secretory lysosomes; co-stimulated exocytosis of recycling endosomes provides a source of additional membrane and may play other roles. Here, we show that a dominant negative form of the recycling endosome protein Rab11 (S25N) interferes with both of these exocytic processes. Inhibition mediated by S25N Rab11 can be bypassed using compounds that block actin polymerization. Furthermore, inhibition of stimulated exocytosis by the F-actin stabilizer, jasplakinolide, is not additive with S25N Rab11, implicating Rab11 in actin remodeling necessary for exocytosis.

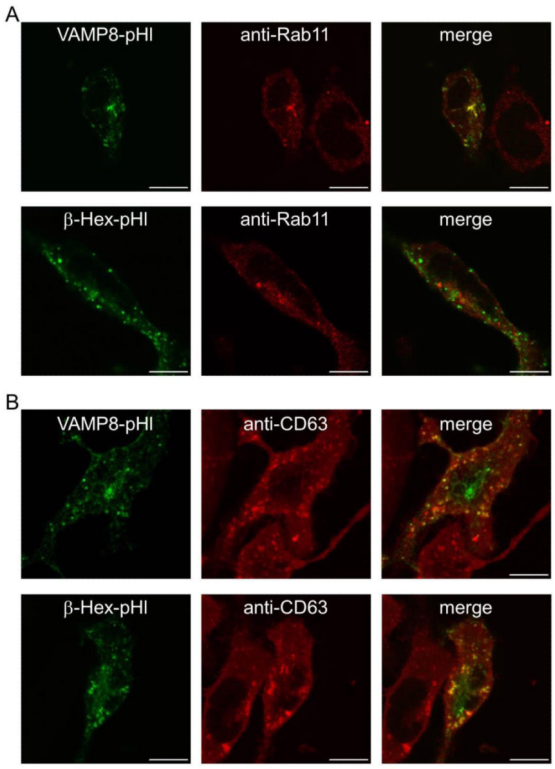

Figure 1. pHluorin-based exocytosis reporters are localized in Rab11-positive endosomes and lysosomes

RBL-2H3 cells were transfected with VAMP8-pHl or β-Hex-pHl, fixed, permeabilized, probed with anti-Rab11 **(A)** or anti-CD63 **(B)** antibodies, and imaged by confocal microscopy. Scale bars are 10 μm. Representative images are shown.

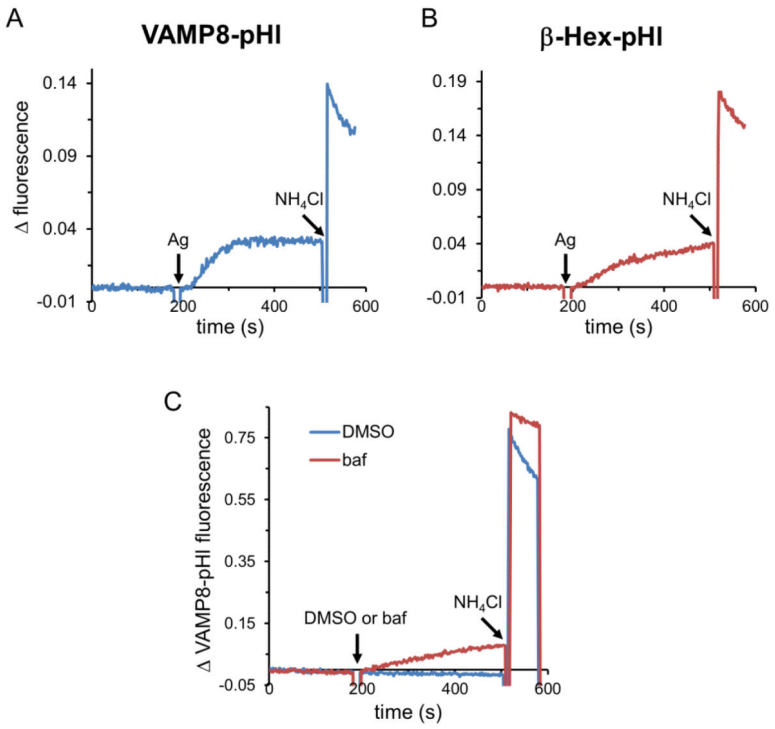

Figure 2. Ag-stimulated exocytosis can be monitored with VAMP8-pHl or β-Hex-pHl reporters

(A) RBL-2H3 cells transfected with VAMP8-pHl and sensitized with anti-DNP IgE were suspended, and fluorescence was monitored spectroscopically. Exocytosis was stimulated by the addition of 100 ng/ml DNP-BSA (Ag), and total fluorophore dequenching was achieved by adding 50 mM NH_4Cl. Raw data were normalized by subtracting baseline fluorescence (t=0) from each subsequent fluorescence value. **(B)** Cells were prepared and analyzed as in (A), except that β-Hex-pHl was transfected instead of VAMP8-pHl. **(C)** 100 nM bafilomycin (baf) or vehicle (dimethyl sulfoxide, DMSO) was added as indicated, and data were normalized as for (A).

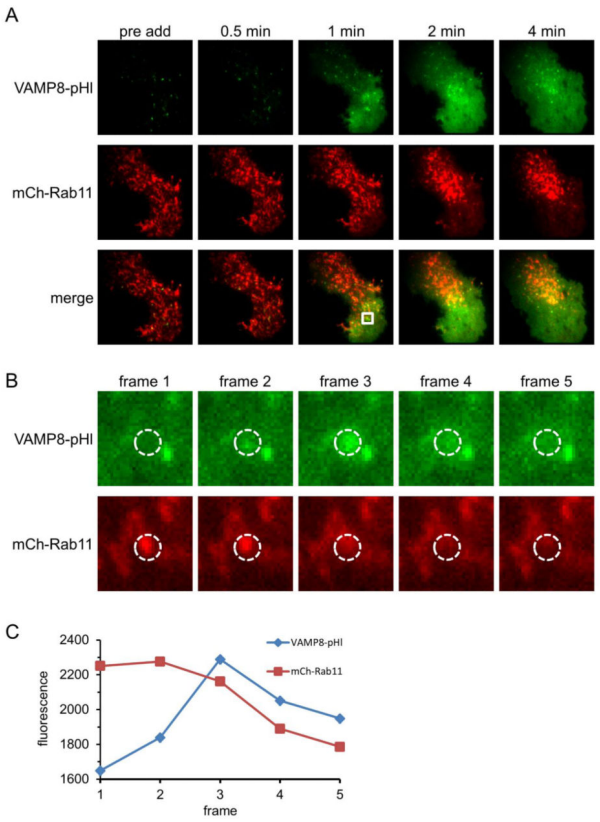

Figure 3. VAMP8-pHl exocytic events are frequently marked by Rab11

RBL-2H3 cells co-transfected with VAMP8-pHl (green) and mCh-Rab11 (red) were visualized by two-color TIRF microscopy and stimulated with 200 ng/ml Ag. **(A)** Individual frames show a cell before Ag addition (pre add) and at various times after Ag addition. **(B)** Individual frames at 1 min post-Ag addition highlighting a mCh-Rab11-labeled vesicle fusing with the plasma membrane, resulting in the dequenching of vesicular VAMP8-pHl fluorescence. Frame 3 is same as 1 min frame from (A). Frame rate is 5.4 fps. **(C)** Integrated fluorescence traces of the region of interest (dashed circles) shown in (B) to quantify coordinated loss of mCh-Rab11 fluorescence and VAMP8-pHl fluorescence dequenching. Image boxes are 25.6 μm^2 in (A) and 3 μm^2 in (B). Scale bars are 5 μm in (A) and 0.6 μm in (B).

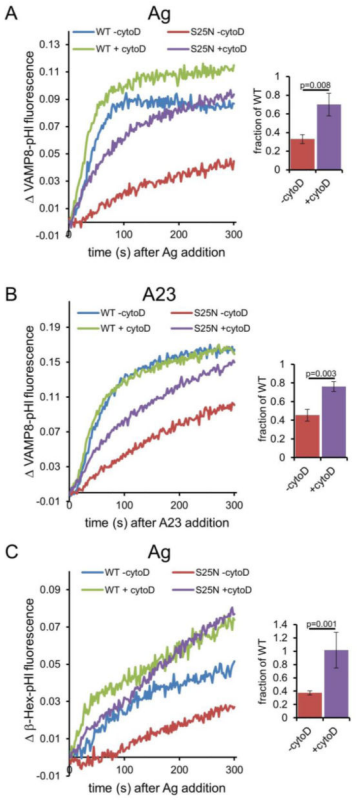

Figure 4. Dominant negative (S25N) Rab11 inhibits stimulated exocytosis monitored by VAMP8-pHl or β-Hex-pHl, which can be rescued by cytochalasin D (cytoD)

(A) RBL-2H3 cells were co-transfected with VAMP8-pHluorin and wild-type (WT) or dominant negative (S25N) mCh-Rab11, and sensitized with anti-DNP IgE (for stimulation with Ag) before harvest. Cells were treated with 2 μM cytoD or vehicle (DMSO, -cytoD) for 5 minutes before exocytosis was stimulated with 100 ng/ml DNP-BSA (Ag). Fluorescence was monitored spectroscopically. Data were normalized as described in Materials and Methods. Bar graph shows integrated fluorescence values expressed as a ratio (S25N/WT) to quantify rescue of S25N Rab11-mediated inhibition by cytoD. **(B)** Cells were prepared and analyzed as in (A) except that 1 μM A23187 (A23) was added in place of Ag. **(C)** Cells were prepared and analyzed as in (A) except that β-Hex-pHl was transfected and monitored instead of VAMP8-pHl. In all cases: the average of three experiments at t=300 s is shown at right, error bars are standard deviations, and p-values were calculated using the unpaired *t*-test.

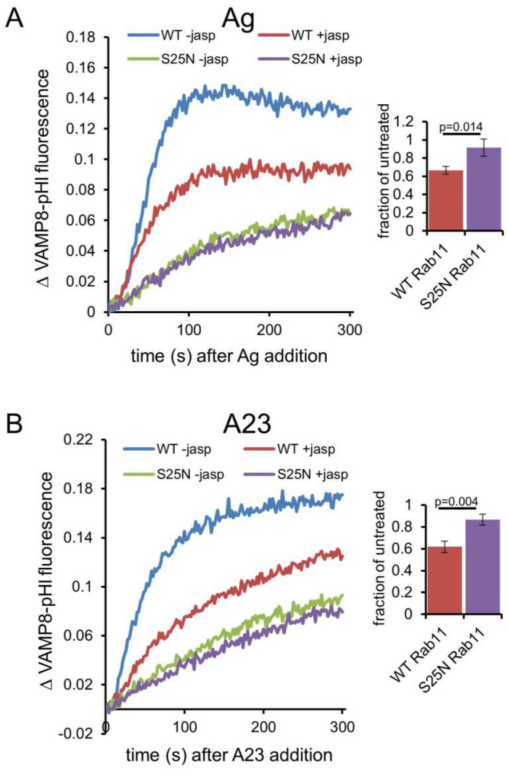

Figure 5. Jasplakinolide (jasp) inhibits stimulated VAMP8-pHl exocytosis

(A) RBL-2H3 cells were co-transfected with VAMP8-pHluorin and either wild-type (WT) or dominant negative (S25N) mCh-Rab11, and sensitized with anti-DNP IgE (for stimulation with Ag) before harvest. Cells were treated with 3 μM jasp or vehicle (DMSO, -jasp) for 5 minutes before exocytosis was stimulated with 100 ng/ml DNP-BSA (Ag). The data were collected and analyzed as in Figure 4. Bar graph shows integrated fluorescence values expressed as a ratio (jasp treated/untreated) to quantify jasp-mediated inhibition of stimulated exocytosis in the context of WT Rab11 but not S25N Rab11. **(B)** Cells were prepared and analyzed as in (A) except 1 μM A23187 (A23) was added instead of Ag. On the right side, the average of three experiments is shown for each condition at t=300 s, error bars are standard deviations, and p-values were calculated using the unpaired *t*-test.

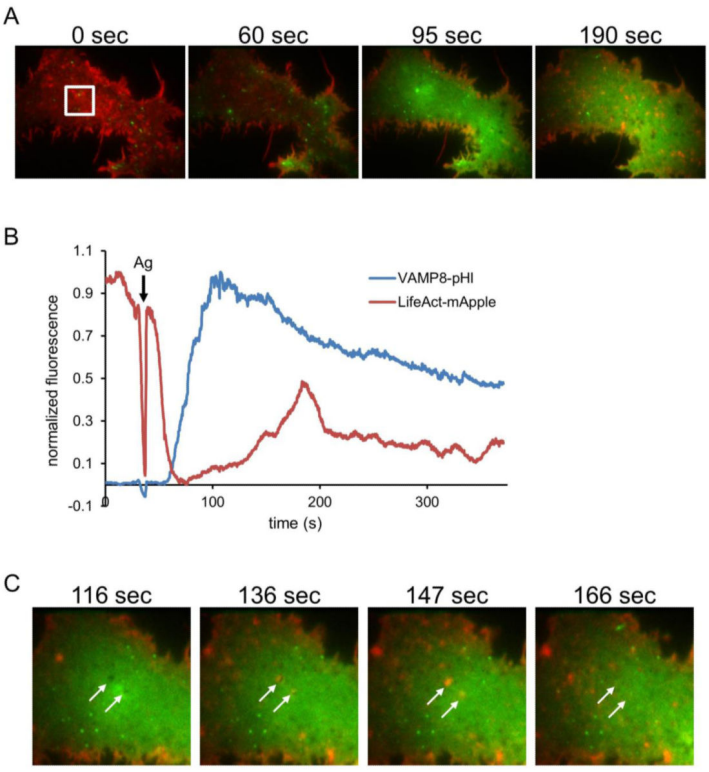

Figure 6. Ag-stimulated exocytosis of VAMP8-pHl is temporally correlated with cortical actin dynamics

RBL-2H3 cells co-transfected with VAMP8-pHl (green) and LifeAct-mApple (red) were visualized by two-color TIRF microscopy and stimulated with 200 ng/ml Ag. A representative cell is shown. **(A)** Individual frames show a cell before Ag addition (0 sec) and at indicated times after Ag addition (Ag added at 35 sec). **(B)** Quantification of the fluorescence intensity in white box shown in (A), normalized by scaling between 0 and 1. **(C)** Individual frames from the same cell in (A) show LifeAct (F-actin) and Vamp8-pHl dynamics after Ag addition, and arrows point to apparent plasma membrane invaginations. Image boxes are 32 × 25 μm in (A) and 16 μm^2 in (C). Scale bar is 8 μm in (A) and 4 μm in (C).

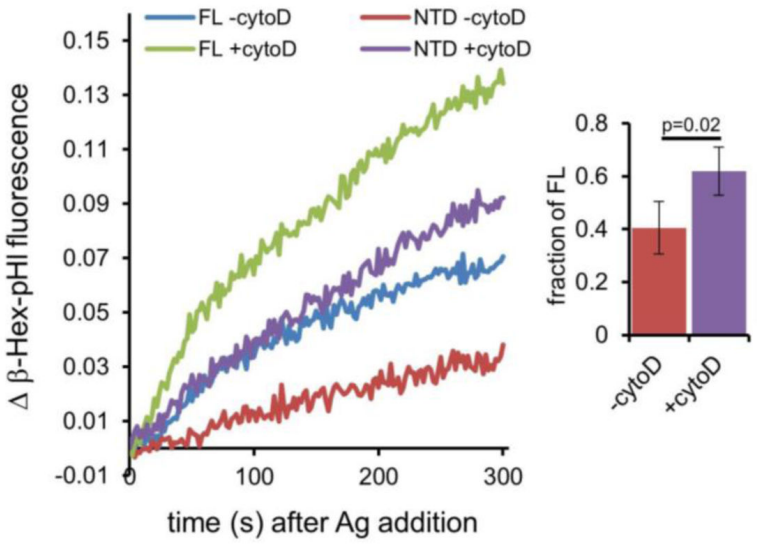

Figure 7. Expression of the p50RhoGAP Sec14 homology domain (NTD) inhibits Ag-stimulated β-Hex-pHl exocytosis

RBL-2H3 cells were transfected with β-Hex-pHl and either full length (FL) or the N-terminal domain (NTD) of p50RhoGAP fused to mCherry and sensitized with anti-DNP IgE before harvest. Fluorescence was monitored by spectroscopy. Cells were treated with 2 μM cytoD or vehicle (DMSO, -cytoD) for 5 minutes before exocytosis was stimulated with 100ng/ml DNP-BSA. The bar graph shows integrated fluorescence values expressed as a ratio (NTD/FL) to quantify rescue of NTD-mediated inhibition by cytoD. The average of four experiments is shown at right for t=300 s, error bars are standard deviations, and the p-value was calculated using the unpaired *t*-test.